INTERNATIONAL JOURNAL FOR NUMERICAL METHODS IN FLUIDS, VOL. 24, 1079–1090 (1997)

A NUMERICAL STUDY OF THE EFFECT OF FREE SURFACE AND WATER DEPTH ON THE STABILITY OF WAKES: USE OF GDQ FORMULATION

Q. D. ZHANG, B. C. KHOO AND K. S. YEO

Department of Mechanical and Production Engineering, National University of Singapore, Singapore 0511, Singapore

SUMMARY

The instability character of a wake in the presence of a free surface is examined by a recently developed GDQ (generalized differential quadrature) numerical method. It is shown that at low Froude number the wake near a free surface is convectively unstable, but when the Froude number is increased further it becomes absolutely unstable. The effect of water depth on the stability property of the wake flow is also investigated. It is found that the influence of water depth on the critical point of instability is limited to at most 20% variation in the complex frequency, while the change in temporal growth rate is also limited to about 20%. © 1997 by John Wiley & Sons, Ltd.

Int. J. Numer. Meth. Fluids, **24**, 1079–1090 (1997)

No. of Figures: 7. No. of Tables: 1. No. of References: 12.

KEY WORDS: wake flow; free surface; instability; GDQ method

1. INTRODUCTION

Many investigators have studied the instability properties of the wake of an object moving in an infinite fluid. Their results reveal that the two-dimensional wake behind both blunt and streamlined bodies is extremely sensitive to the external excitation. However, the instability characteristics of the near- and far-wake flows are quite different. The two-dimensional wake immediately behind an object is always absolutely unstable, whereas the wake far away from the object is convectively unstable.[1–4]

Recently, in an effort to study the stability of the deformation of the ocean surface resulting from interaction with a submerged vorticity field, Triantafyllou and Dimas[5] investigated the instability property of a floating or half-submerged body. For the situation of low Froude number they considered the initial separated flow past a floating object (in the shape of a hydrofoil and a circular cylinder) as one-half of the 'double-body' flow. Using the measured wake velocity profile behind an object in an infinite medium, they imposed on the shear-free condition on the symmetric half of the profile to simulate the presence of a free surface and studied the resulting property of the wake flow. Their results show that at low Froude number the wake immediately behind a 'floating' two-dimensional object is convectively unstable. Beyond a certain value of Froude number, however, it becomes absolutely unstable. When the Froude number is very large, the instability character approaches the case of submergence in an infinite fluid. This result indicates that the presence of a free surface can drastically alter the instability properties and large-scale unsteady patterns in two-dimensional wakes. At low Froude number the presence of a free surface has a stabilizing effect, suppressing somewhat the unsteadiness of the wake. At high enough Froude number, large-amplitude waves appear that cause the instability of the wake to become absolute.

CCC 0271–2091/97/111079–12 $17.50

Received February 1995
Revised April 1996

In this work the instability of wake flows near a free surface[5] is re-examined using a recently developed numerical method, the generalized differential quadrature (GDQ) procedure of Shu and Richards.[6] The GDQ method is a finite-difference-based scheme derived from a method of differential quadrature proposed by Bellman *et al.*[7] Compared with standard finite difference discretization in which the order of approximation is normally much less than the number of grid points, the GDQ method is optimum in the sense that it achieves the highest possible order of approximation for a given number of grid points. Thus for a given order of accuracy the GDQ method requires much fewer grid points than the standard second- and fourth-order finite difference schemes. In practice the GDQ method is only limited by the truncation error of floating point arithmetic operations. The small number of grid points required to attain a specified order of accuracy ultimately translates into a vast saving in computing time and storage, which is borne out in our calculations.

Besides verifying the findings of Triantafyllou and Dimas,[5] which were based on a second-order finite difference approximation, and demonstrating the efficiency/superiority of the GDQ method, the present paper also investigates the influence of water depth on the stability of the wake profiles of a hydrofoil and a circular cylinder. It is found that for the wakes following a hydrofoil the water depth has little influence on the nature of the instability as the critical point of instability has at most 20% variation in the complex frequency as the depth decreases from infinity. The temporal growth rate also appears to have limited variation as the water depth is reduced. These observations are equally valid for the wake flow due to a circular cylinder, which may suggest a limited effect of depth on the stability properties of wake flows in the presence of a free surface.

2. MATHEMATICAL FORMULATION OF THE INSTABILITY PROBLEM

2.1. Flow stability

We choose a Cartesian co-ordinate frame for the problem as follows: the positive x-axis is directed from left to right and lies along the initially undisturbed surface of the water; the positive y-axis points vertically upwards. The fluid is assumed to be incompressible and inviscid. We denote the two-dimensional parallel primary/basic velocity field by $(U(y), 0)$. A small-amplitude normal mode perturbation is added to the basic mean flow $U(y)$, which has the form $(u, v) = (\partial/\partial y, -\partial/\partial x)\phi(y)\exp[\mathrm{i}(kx - \omega t)]$. Here ω and k represent the complex frequency and complex wave number of the perturbation respectively. The disturbance function $\phi(y)$ obeys the well-known Rayleigh equation,[8] i.e.

$$(kU - \omega)(\phi'' - k^2\phi) - kU''\phi = 0, \quad y < 0. \tag{1}$$

Here a superscript prime denotes the ordinary derivative taken with respect to y. The normal component of velocity is set to zero on the solid bottom surface. Hence

$$\phi(y) = 0 \quad \text{at } y = -h, \tag{2}$$

where h is the water depth measured from the free surface.

Let $\eta(x, t) = \hat{\eta}\mathrm{e}^{\mathrm{i}(kx-\omega t)}$ denotes the displacement of the free surface resulting from the perturbation. The free surface boundary conditions are the continuity of normal velocity and pressure. The linearized forms of these conditions are

$$(\omega - kU_{\mathrm{w}})\hat{\eta} = k\phi_{\mathrm{w}}, \tag{3}$$

$$(kU_{\mathrm{w}} - \omega)\phi'_{\mathrm{w}} - kU'_{\mathrm{w}}\phi_{\mathrm{w}} = -\hat{p}_{\mathrm{w}}, \tag{4}$$

where $\hat{p}_w$ is the complex amplitude of pressure perturbation at $y = 0$. The subscript 'w' denotes evaluation at $y = 0$. We further note from the dynamic balance of forces at the mean free surface that

$$\hat{p}_w = g\hat{\eta}, \tag{5}$$

where g is the acceleration due to gravity. Combining equations (3)–(5), we have

$$Fr^2(kU_w - \omega)^2\phi'_w - k^2\phi_w = 0, \tag{6}$$

where $Fr = U_\infty/\sqrt{(gb)}$ is the Froude number and the no-shear free surface boundary condition has been used. The above equations are considered as having been non-dimensionalized with respect to the infinite freestream velocity U_∞ for velocity and the half-width of the wake, b, for linear dimension of length.

The Rayleigh equation (1), the solid surface boundary condition (2) and the free surface boundary condition (6) constitute a closed system of homogeneous equations that governs the stability of the mean flow $U(y)$.

2.2. The Generalized Differential Quadrature method

Equations (1), (2) and (6) can be cast into the form of a generalized eigenvalue problem for a given k with ω as an eigenvalue and ϕ as an eigenfunction. There exist many schemes which can be used to discretize the above equations. Here we have chosen the GDQ method.

The GDQ method[6] expresses the derivatives of the unknown function $\phi(y)$ (assumed to be sufficiently differentiable) as linear combinations of the values of the functions at the grid points. Thus for a second-order ordinary differential equation we can write

$$\phi_y(y_i) = \sum_{j=1}^{N} a_{ij}\phi(y_j), \tag{7}$$

$$\phi_{yy}(y_i) = \sum_{j=1}^{N} b_{ij}\phi(y_j), \tag{8}$$

where $\phi_y(y_i)$ and $_{yy}(y_i)$ denote the first- and second-order derivatives of $\phi(y)$ respectively at the grid points $\{y_i, i = 1, \ldots, N\}$.

A smooth function can always be represented to any order of accuracy in terms of polynomial functions from any complete polynomial basis. The weighting coefficients are determined from this knowledge by requiring that the selected polynomials from the basis satisfy the representations (7) and (8), interpreted as linear constraint relationships. Various polynomial bases may be used. The employment of Legendre and Chebyshev polynomials results in determinations for a_{ij} and b_{ij} which are subject to a restriction on the co-ordinates of the grid points. The use of Lagrange interpolation polynomials, which is the basis of the GDQ method, allows complete freedom on the choice of grid points y_i, which makes the method particularly useful. The use of Lagrange interpolation polynomials results in the following determination for the weighting coefficients. The weighting coefficients a_{ij} for the first-order derivative are given by

$$a_{ij} = \frac{M^{(1)}(y_i)}{(y_i - y_j)M^{(1)}(y_j)} \quad \text{for } j \neq i, \tag{9}$$

$$a_{ii} = -\sum_{j=1.j\neq i}^{N} a_{ij} \quad \text{for } j = i, \tag{10}$$

where

$$M^{(1)}(y_i) = \prod_{j=1, j\neq i}^{N} (y_i - y_j). \tag{11}$$

The weighting coefficients b_{ij} for the second-order derivative are given by

$$b_{ij} = 2a_{ij}\left(a_{ii} - \frac{1}{y_i - y_j}\right) \quad \text{for } j \neq i, \tag{12}$$

$$b_{ii} = -\sum_{j=1, j\neq i}^{N} b_{ij} \quad \text{for } j = i. \tag{13}$$

From the expressions for the coefficients a_{ij} and b_{ij} it is apparent that the GDQ method utilizes all the information contained in the grid function $\phi(y_i)$ in obtaining the respective derivatives. Hence in this way the said method can be considered as a variant of the finite difference method (FDM), with the highest possible order of accuracy (depending on the number of grid points used). Since the GDQ method is a highly accurate scheme, it permits the use of greatly reduced number of grid points to achieve a given level of numerical accuracy. It is this advantage that makes the use of GDQ method attractive in solving the present problem. The reader is referred to Reference 6 for further details.

2.3. Dispersion relation

To cast the Rayleigh equation (1) and the boundary conditions (2) and (6) in the form of a matrix linear eigenvalue problem in ω, we rewrite the free surface boundary condition (6) as

$$Fr(kU_w - \omega)A - k^2\phi_w = 0, \quad y = 0, \tag{14}$$

$$Fr(kU_w - \omega)\phi'_w = A, \quad y = 0. \tag{15}$$

This reformulation allows us to avoid the term ω^2 in the original free surface boundary condition (6) (which would prevent the formation of the linear eigenvalue problem) at the expense of introducing an unknown constant A which is solved as part of a matrix eigenvalue problem.

Using the GDQ scheme to discretize the governing Rayleigh equation (1) and the boundary conditions given in (14) and (15) results in the matrix (dispersion) equation

$$D(k, \omega) \equiv ([\mathbf{A}] - \omega[\mathbf{B}])(A, \phi_1, \phi_2, \ldots, \phi_N)^{\mathrm{T}} = 0, \tag{16}$$

where[$\mathbf{A}$] and [$\mathbf{B}$] are complex matrix functions of the wave number k and the velocity profile U_j and ϕ_i $(i = 1, 2, \ldots, N)$ are the values of the eigenfunction $\phi(y)$ at the grid points of the mesh covering the flow domain. The eigenvalues ω and their corresponding eigenvectors $\{A, \phi_i, \ldots, \phi_N\}^{\mathrm{T}}$ for prescribed velocity profile and complex wave number k may be obtained numerically by the standard Q–Z algorithm without the need for any guess values. In this the present method has the advantage over the standard shooting procedures which generally requires some prior knowledge of the eigenvalues. An extensive search or trial-and-error scheme may have to be instituted when such prior knowledge is absent. For problems where most of the eigenvalues represent damped eigenstates ($\omega_i < 0$), the matrix eigenvalue method will generally allow all the unstable eigenstates to be located. With shooting methods it is difficult to be certain that all the unstable modes have been found. The disadvantage is that the computational effort involved is greater for the matrix eigenvalue method. However, since the identification of instabilities is the *raison d'être* for stability studies, the matrix approach is much to be preferred if computing resource is not an overriding limitation.

2.4. Spatial–temporal instabilities

In the context of linear stability theory the unstable space–time evolution of an unstable disturbance mode is described by the Green function defined by

$$G(x,t)=\int_L \mathrm{d}\omega \frac{\mathrm{e}^{-\mathrm{i}\omega t}}{2\pi}\int_F \mathrm{d}k \frac{\mathrm{e}^{\mathrm{i}kx}}{2\pi}\frac{1}{D(k,\omega)}, \tag{17}$$

where $D(k,\omega)=0$ is the dispersion relation. The integrations in the Laplace–Fourier integral (17) must be carried out on contours placed in the domains of absolute convergence of the complex frequency ω-plane and complex wave number k-plane. The stability character is determined by deforming (lowering) the Laplace contour L towards the ω_r-axis. The Fourier contour F is concomitantly adjusted (deformed) when necessary within its domain of absolute convergence to separate the $k(\omega_\mathrm{L})$-roots which originate from opposite (top and bottom) halves of the k-plane, in order to preserve the analyticity of the ω-integrand

$$I(x,\omega)=\int_F \frac{\mathrm{d}k}{2\pi}\frac{\mathrm{e}^{\mathrm{i}kx}}{D(k,\omega)}. \tag{18}$$

The deformation of the F-contour to preserve the analyticity of I is inhibited, however, when two k-roots originating from opposite halves of the k-plane coalesce (intersect). Such coalescence, which 'pinches' the F-contour at the root coalescence point, produces a singularity in I. When such a singularity occurs, which effectively prevents the L-contour from being deformed completely onto the ω_r-axis, we have an absolute instability, which is an instability that grows in time at all points in space, i.e.

$$\lim_{t\to\infty} G(x,t)\to\infty \quad \text{for all fixed } x. \tag{19}$$

Otherwise, there is at most convective instability, which is an instability that propagates in one direction as it grows, so that at any fixed point x the disturbance ultimately decays to zero, i.e.

$$\lim_{t\to\infty} G(x,t)\to 0 \quad \text{for all fixed } x. \tag{20}$$

A detailed account of the theory is given by Bers.[9]

Kupfer *et al.*[10] developed a useful procedure for identifying absolute instability. The procedure is based upon the mapping of constant k_i-contours into the ω-plane through the dispersion relation. The occurrence of a cusp-like point in the ω-plane indicates the existence of a double k-root (or root coalescence), which is a necessary but not sufficient condition for the existence of a 'pinch point' and absolute instability. The identification of a 'pinch point' or absolute instability is made by further counting the number of times the ω-contour of $k_\mathrm{i}=0$ intersects the vertical line $\omega_\mathrm{r}=\text{constant}$ drawn vertically upwards from the estimated location of the branch cusp point. An odd number of intersections indicates a genuine pinch point and therefore an absolute instability mode. Convective instabilities, on the other hand, are given by causal spatially growing (upstream or downstream) eigenmodes for real eigenfrequencies. They may be identified by the intersection of $k_\mathrm{i}<0$ contours with the ω_r-axis (i.e. $\omega_\mathrm{i}=0$) in the ω-plane. The causality condition is realized if a vertical line (i.e. $\omega_\mathrm{r}=\text{constant}$) drawn vertically upwards from the intersection point cuts the $k_\mathrm{i}=0$ contour in the ω-plane an odd number of times.

3. RESULTS AND DISCUSSION

3.1. Comparison with previous work: GDQ and FDM approach

In the absence of any measured or theoretical wake velocity profile of a half-submerged hydrofoil positioned at the air–water interface, the velocity profile of a thin symmetrical NACA 0003 hydrofoil obtained experimentally by Mattingly and Criminal[2] in an infinite fluid is adopted with the proviso that the free surface conditions be applied at the point of symmetry of the said velocity profile. Since the time-averaged wake velocity distribution of a hydrofoil (or any object) as affected by the vortex street—hence implying that there will be differences in the time-averaged flow properties in the wake of a floating hydrofoil when compared with an infinite fluid—one should view the results of a stability test on the effect of a free surface qualitatively for possible inference of the true wake on a moving floating body. In this section we shall only consider the case of an infinite (or very large) water depth.

As stated by Triantafyllou and Dimas,[5] the near-wake velocity profile measured by Mattingly and Criminal[2] is given as

$$U(y) = U_\infty - (U_\infty - U_c)\frac{1}{\cosh^2(\sigma y)}, \quad -\infty < y < 0, \tag{21}$$

where the centreline velocity U_c is taken as 0·0012 as the streamwise location behind the trailing edge of the hydrofoil at $x = 0{\cdot}003l$ (l being the length of the NACA 0003 hydrofoil) and $\sigma = 0{\cdot}88137$. (All linear dimensions are non-dimensionalized with respective to b, the half-width of the wake.) The infinite water depth is simulated nominally at $y = -8b$. It may be noted that the flow profile has one inflection point and is strongly unstable; to be more precise, it exhibits absolutely unstable behaviour in an unbounded fluid.[2,4] For the wake profile (21), results of k_i-contours in the comples ω-plane, computed using the GDQ algorithm for $Fr = 5{\cdot}5$, are shown in Figure 1. The results shown belong to branch 2 instability; branch 1 results are stable for this case. The distribution of the k_i-contours is

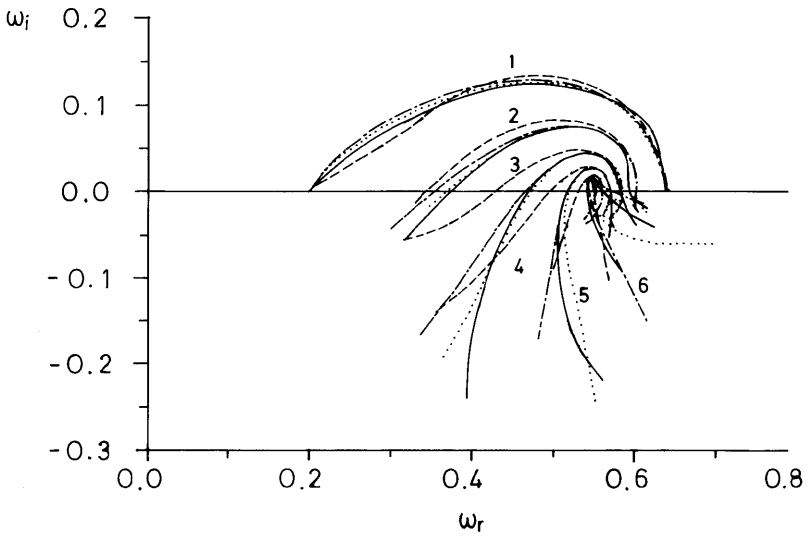

Figure 1. Instability curves for hydrofoil at $Fr = 5{\cdot}5$ and different water depths: curves 1–6, branch 2, $k_i = 0, -0{\cdot}2, -0{\cdot}4, -0{\cdot}6, -0{\cdot}8, -1{\cdot}0$; ——, $h = 8$; ·····, $h = 4$; – · –, $h = 3$; – – – –, $h = 2$

closely identical with results obtained using the regular grid, second-order, three-point FDM (not shown) and concurs with similar FDM result of Dimas.[11] The presence of a cusp point with $\omega_i > 0$, and which also satisfies the intersection criterion, indicates the existence of absolute instability.

Table I compares the ω-eigenvalues of an unstable eigenstate close to the cusp point in Figure 1, calculated using the second-order FDM on a regular interval mesh and the GDQ method on a Chebyshev–Gauss–Lobatto distribution mesh with different numbers of grid points. The CPU timings are also given. (The calculation is carried out on a DEC 7000/610 machine and the CPU time is obtained by utilizing the subroutine X05BAF of the NAG Library.) For $N=50$ the GDQ method requires about 50% more processing time than the FDM for the determination of all the ω-eigenvalues. (Only the unstable eigenvalues, of which there is just one, are given in Table I.) This is not surprising, because the GDQ method requires more arithmetic operations to set up the coefficient matrix. The GDQ method is, however, much more accurate, as a comparison with the reference eigenvalue $\omega = 0{\cdot}54853 + i0{\cdot}01576$ will show; the reference value was calculated using a highly accurate shooting procedure. The GDQ result with $N=50$ is slightly more accurate than the FDM result with $N=400$, but requires much less CPU time, a ratio of close to 380. Granted that the FDM approach has to process many more eigenvalues (since the Q–Z algorithm solves for all the eigenvalues of the dispersion matrix equation), the ratio of CPU times per eigenvalue still works out to be a factor of about 50 in favour of the GDQ method. The large number of eigenvalues obtained by the FDM is not an advantage, because the unstable eigenmodes, which are important eigenmodes, can generally be detected even with fairly modest values of N. Large N merely allows the unstable eigenmodes to be obtained with greater accuracy. For a comparable level of accuracy in the results, say GDQ with $N=50$ and FDM with $N=400$, the GDQ method also requires considerably smaller processing memory because of the smaller size of the matrix involved. Incidentally, our results for FDM with $N=200$ and GDQ with $N=30$ are in agreement for the same eigenvalue to the three decimal digits quoted by Dimas.[11] For the GDQ method we may also note that the increase in CPU time is roughly linear with N, whereas for the FDM the growth is much more rapid.

Further computations of the instability plots of ω_i versus ω_r at different k-contours for Fr ranging from 0·5 to 5·5 in intervals of 1·0 were carried out using both the FDM based on 200 grid points and GDQ with a nominal 50 grid points. The general distributions in the ω-plane for given values of k show similar features to those of Reference 11 (not shown). For $Fr \leqslant 1{\cdot}5$, two branches of instability are detected, one occurring at low wave number (called branch 1 as in Reference 11) which is close to the varicose mode in an infinite fluid and the other occurring in the higher-wave-number region

Table I. Comparison of results and CPU times between regular grid, second-order FDM and non-regular grid GDQ method. The ω-eigenvalue given corresponds to the cusp point in Figure 1. $Fr = 5{\cdot}5$, $k_r = 1{\cdot}2$, $k_i = -1{\cdot}0$

Method	Grid points	Result (ω)	CPU time (s)	CPU time (s) per eigenvalue
FDM	$N=50$	$\omega_r = 0{\cdot}54497$, $\omega_i = 0{\cdot}01238$	0·2176	0·00435
	$N=100$	$\omega_r = 0{\cdot}54803$, $\omega_i = 0{\cdot}01557$	1·453	0·01453
	$N=200$	$\omega_r = 0{\cdot}54847$, $\omega_i = 0{\cdot}01577$	12·324	0·06162
	$N=300$	$\omega_r = 0{\cdot}54851$, $\omega i = 0{\cdot}01578$	46·413	0·15471
	$N=400$	$\omega_r = 0{\cdot}54852$, $\omega_i = 0{\cdot}01577$	122·412	0·30603
GDQ	$N=16$	$\omega_r = 0{\cdot}53962$, $\omega_i = 0{\cdot}01629$	0·126	0·00788
	$N=20$	$\omega_r = 0{\cdot}55044$, $\omega_i = 0{\cdot}01533$	0·153	0·00765
	$N=30$	$\omega_r = 0{\cdot}54872$, $\omega_i = 0{\cdot}01552$	0·163	0·00543
	$N=40$	$\omega_r = 0{\cdot}54854$, $\omega_i = 0{\cdot}01571$	0·241	0·00603
	$N=50$	$\omega_r = 0{\cdot}54853$, $\omega_i = 0{\cdot}01575$	0·324	0·00648

(known as branch 2, like the sinuous mode in an infinite fluid for supercritical flows). Careful examination of the critical points at ω_{0i} in the ω-plane shows good general agreement of the critical point as a function of the Froude number between GDQ and the FDM: for branch 2 the agreement of critical points is identical up to three decimal digits, while the concurrence of results for branch 1 instability is within 5%. Further comparison is carried out for the maximum temporal growth rate $(\omega_i)_{max}$ (not shown). The maximum temporal growth rate is the maximum value of ω_i for the $k_i = 0$ contour in the ω-plane. The computed results of $(\omega_i)_{max}$ using the GDQ method and the FDM show that agreement of the maximum temporal growth rate is up to at least three decimal digits and this occurs for both branches of the instability curves. Overall, the computations using GDQ and the FDM yield fairly similar results, which in turn compare very well with Diamas's results. This clearly establishes GDQ as an alternative numerical method which promises a vast saving of computational effort for the study of linear stability analysis.

Dimas further evaluated the stability of a cylinder wake by using the velocity profile of an unbounded flow around the cylinder at a Reynolds number (based on the freestream velocity and the diameter of the cylinder) of 140,000 obtained experimentally by Cantwell.[12] The said experimental data were curved fitted by Triantafyllou *et al.*[4] as follows:

$$U(y) = 1 - A[1 - \tanh(\alpha y^2 - \beta)], \quad -\infty \leqslant y \leqslant 0. \tag{22}$$

Here the velocity profile at the streamwise location behind the cylinder at $x/d = 1$ (where d is the diameter of the cylinder), which corresponds to $A = 0{\cdot}75$, $\alpha = 0{\cdot}68162$ and $\beta = 0{\cdot}32$, was adopted for the study. (A, α and β are curve-fitting parameters.) The vertical co-ordinate is non-dimensionalized with respect to b, the half-width of the cylinder wake. The 'infinite' depth is simulated at four cylinder diameters d, equivalent to $9{\cdot}7b$ beneath the free surface. As in the previous case, the effect of a free surface with the boundary condition given in (6) is imposed at the point of symmetry of the cylinder wake profile. Our computations using the GDQ approach with a nominal 50 grid points yield the typical distribution of ω_i versus ω_r for different contours of k_i at a Froude number of $1{\cdot}5$ shown in Figure 2. The plots depict a general distribution of both branch 1 and 2 instability curves similar to that obtained by Dimas. The cusp point in the ω-plane indicates the presence of a critical point whose temporal growth rate is denoted by ω_{0i}. Figure 3 shows the variation in ω_{oi} as a function of the Froude number. The distribution of ω_{0i} for the case of 'infinite' water depth compares generally well with the results of Dimas obtained using the FDM. For branch 2, agreement with Dimas's results in exact up to three decimal digits, while in branch 1, our ω_{0i} concurs to within 5%. Figure 3 shows that ω_{0i} is positive for $Fr > 2{\cdot}6$, implying that the instability is absolute in nature for these flows. For smaller Froude numbers the flow is at most convectively unstable. Results for maximum temporal growth rate $(\omega_i)_{max}$ as a function of Fr are shown in Figure 4; $(\omega_i)_{max}$ is positive throughout. For $Fr \leqslant 0{\cdot}5$ the maximum temporal growth rate comes from branch 1, while for larger Fr, $(\omega_i)_{max}$ has its origin in branch 2.

Overall, we have demonstrated the efficiency and superiority of the GDQ method over the standard second-order FDM in the study of the linear stability analysis of wake flow near a free surface. The GDQ method yields results of comparable accuracy to the second-order FDM at a small fraction of computing resources. GDQ is used in the next section to analyse in greater detail the effect of depth on the stability of the wake flows examined above.

3.2. Effect of water depth on the linear stability of wake flow

In the absence of any experimental data or analytical result determining the wake velocity profile in the presence of a free surface and *finite* depth, it is assumed that the near-wake velocity profile of a hydrofoil as expressed in equation (21) is applicable. The boundary condition at the solid bottom is

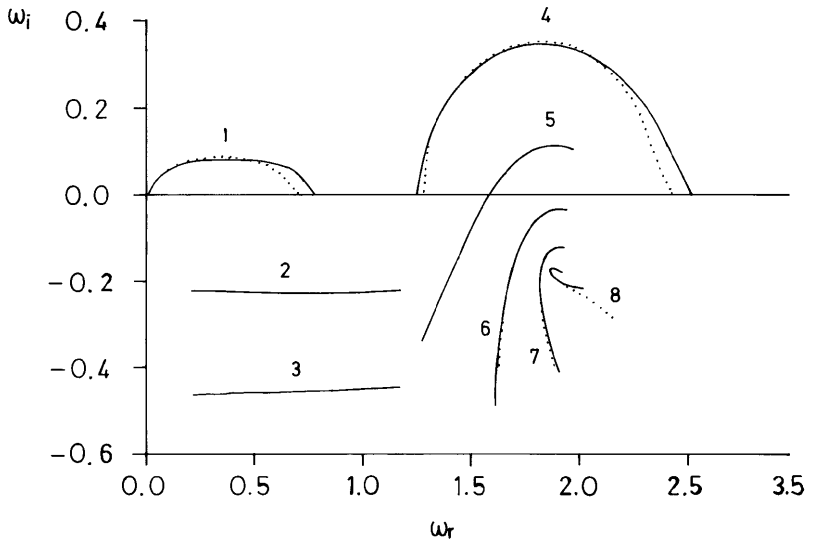

Figure 2. Instability curves for circular cylinder at $Fr = 1{\cdot}5$ and different water depths: curves 1–3, branch 1, $k_i = 0,\ -0{\cdot}7,\ -1{\cdot}4$; curves 4–8, branch 2, $k_i = 0,\ -0{\cdot}7,\ -1{\cdot}4,\ -2{\cdot}1,\ -2{\cdot}8$; ——, $h = 9{\cdot}7$; ·····, $h = 4{\cdot}8$

that the normal component of velocity perturbation be zero, i.e. equation (2). Provided that the latter boundary condition is applied at sufficient depth from the free surface so that the mean wake velocity value is still limited to at least, say, 90% of that at infinite depth, which is equivalent to dimensionless depth $h(\equiv h'/b) \geqslant 2$, where b is the half-width of the wake, it is reckoned that the present analysis may provide some idea of the effect of finite depth on the nature of the wake flow instability.

For $Fr = 5{\cdot}5$ with dimensionless depths $h = 4$, 3 and 2 the distribution of ω_i versus ω_r for different contours of k_i are plotted in Figure 1 for the purpose of comparison with the case of 'infinite' depth. It is quite apparent that while the said distributions of given k_i and different h maintain the same general shape, the distributions are definitely not identical. For the case of $h = 8$ and 4, while the contours of

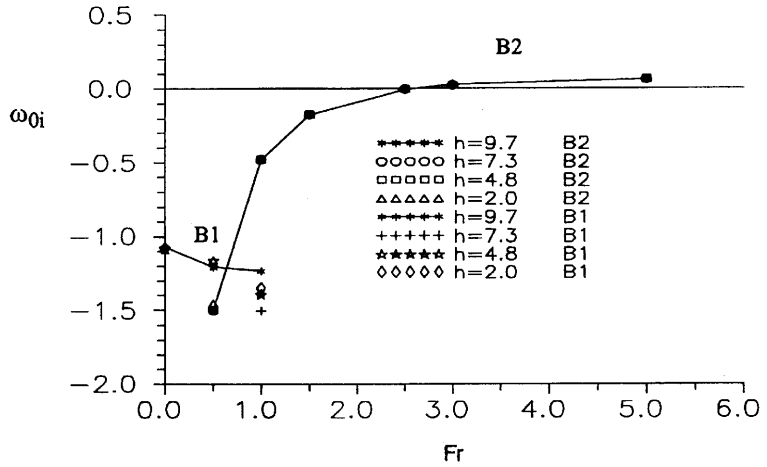

Figure 3. Temporal growth rate at critical point versus Froude number for circular cylinder velocity profile at different water depths for branch 1 and 2 instabilities. The line is drawn through results pertaining to $h = 9{\cdot}7$ (or dimensional depth $4d$)

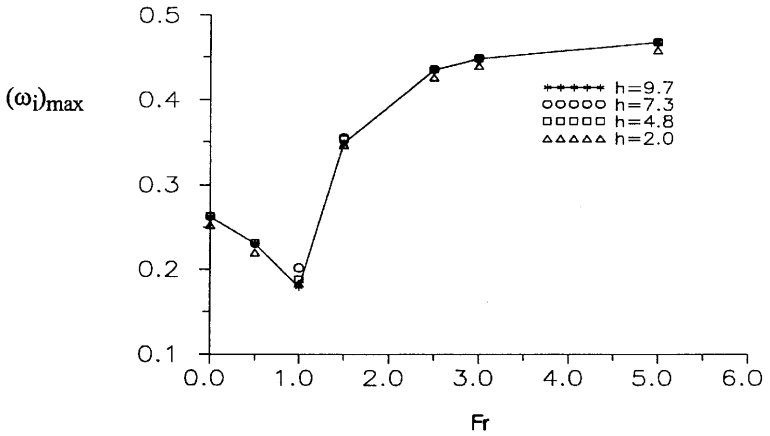

Figure 4. Maximum temporal growth rate versus Froude number for circular cylinder velocity profile at different water depths. The line is drawn through results pertaining to $h=9{\cdot}7$ (or dimensional depth $4d$)

$k_i=0$ and $-0{\cdot}2$ are very close, the differences become more notable for smaller k_i. However, despite the differences in the distribution, the cusp point which indicates the presence of a critical point as denoted by ω_{0i} does not differ very much; numerically, ω_{0i} is given by 0·015815 and differs by less than 1% from 0·015752 at $h=8$. On comparing the infinite depth with the even shallower depths $h=3$ and 2, there is an increasingly greater difference in the distribution of constant k_i, with ω_{0i} becoming slightly less positive; numerically, ω_{0i} at $h=2$ differs by about 15%.

For the other tests carried out in the range of $Fr=4{\cdot}5$–$0{\cdot}5$, decreasing in intervals of 1·0, it is found that the general shape of the constant k_i-contours pertaining to $h=4$, 3 and 2 bears some resemblance to the case of $h=8$, with more differences detected for the smaller h. It is also found that the critical point ω_{0i} did not differ much between $h=8$ and 4, with at most a variation of less than 5%; the

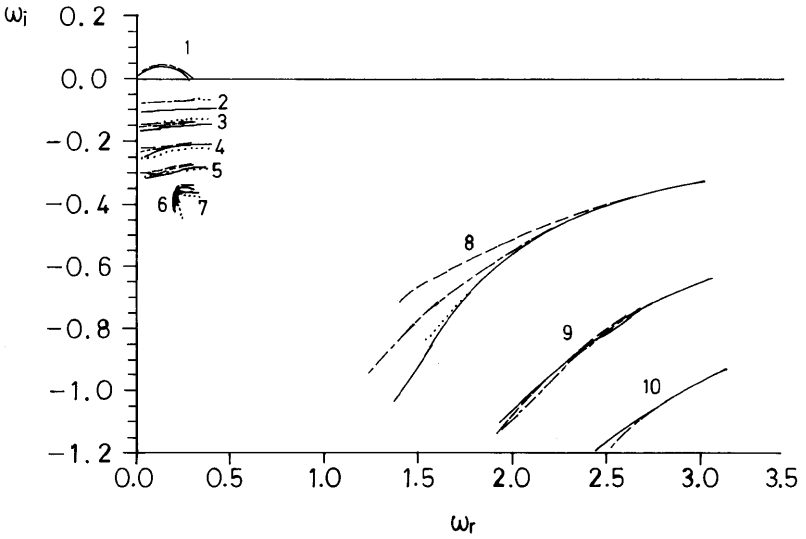

Figure 5. Instability curves for hydrofoil at $Fr=0{\cdot}5$ and different water depths: curves 1–7, branch 1, $k_i=0$, $-0{\cdot}5$, $-1{\cdot}0$, $-1{\cdot}5$, $-2{\cdot}0$, $-2{\cdot}5$, $-2{\cdot}6$; curves 8–10, branch 2, $k_i=-0{\cdot}5$, $-1{\cdot}0$, $-1{\cdot}5$; ——, $h=8$; ·····, $h=4$; –·–, $h=3$; – – – –, $h=2$

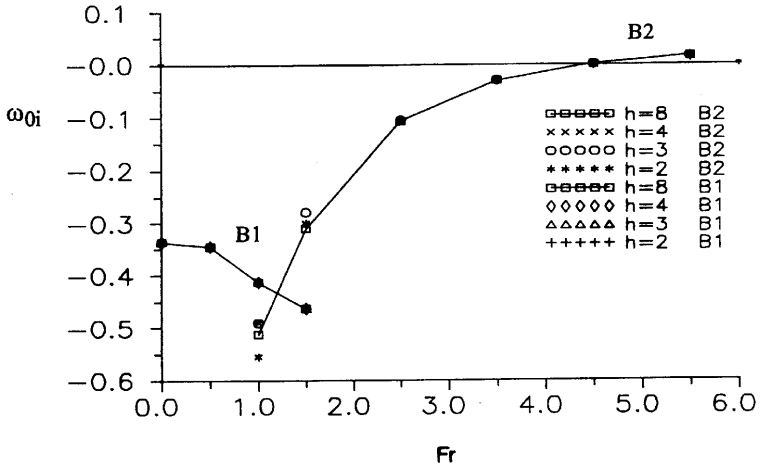

Figure 6. Temporal growth rate at critical point versus Froude number for hydrofoil velocity profile at different water depths for branch 1 and 2 instabilities. The line is drawn through results pertaining to $h = 8$

variation between $h = 8$ and 2 is greater but is still within a band of less than 20%, without any discernible trend. The above observation is also true for branch 1 of the ω_i–ω_r stability plot, as shown for $Fr = 0{\cdot}5$ with $h = 8$, 4, 3 and 2 in Figure 5. Although the constant k_i-contours of different h maintain a generally similar shape, the differences in the detailed distributions have resulted in only slightly different values of the critical point ω_{0i}. A summary of the effect of different depth h on the critical ω_{0i} with respective to Fr is shown in Figure 6. This proves a clear indication that the depth has a somewhat limited influence on the nature of the wake stability of a 'half-submerged' hydrofoil. In Figure 7 the maximum temporal growth rate $(\omega_i)_{max}$ versus Fr for different h is shown. Again the influence of depth on $(\omega_i)_{max}$ is fairly limited, with differences from the value pertaining to 'infinite' depth of less than 20%.

Further tests are carried out to evaluate the effect of depth on the stability of the wake flow of a cylinder in the presence of a free surface. The effect of finite depth is simulated at dimensional heights $h' = 3d$, $2d$ and $0{\cdot}84d$, equivalent to $7{\cdot}3b$, $4{\cdot}8b$ and $2{\cdot}0b$ respectively, beneath the free surface

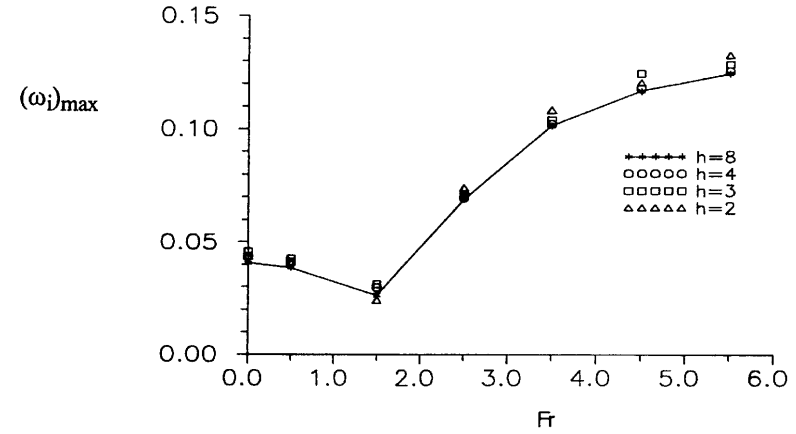

Figure 7. Maximum temporal growth rate versus Froude number for hydrofoil velocity profile at different water depths. The line is drawn through results pertaining to $h = 8$

for comparison with the 'infinite' depth set at $h' = 4d$ (or 9·7b). A typical plot of ω_i versus ω_r for $Fr = 1{\cdot}5$ is shown in Figure 2 for $h = 4{\cdot}8$ for comparison with the 'infinite' depth case taken to be $h = 9{\cdot}7$. It is clear that while there are some differences in the constant k_i-contours their general shapes are still similar and there is only a small variation in the critical point. Fairly similar behaviour of the ω_i–ω_r distribution for different Froude numbers at different depths is also noted (not shown), culminating in the evaluation of critical points which only differ from at infinite depth by less than about 15%; see Figure 3. Results of the maximum temporal growth rate $(\omega_i)_{max}$ for various Fr at different h are shown in Figure 4, which depict changes of less than 10% from that at 'infinite' depth. These results suggest that the effect of depth on the instability of the wake flow behind a cylinder in the presence of a free surface is generally mild.

4. CONCLUSIONS

The present work applies the recently developed method of generalized differential quadrature (GDQ) to the solution of the stability problem of wake flows near a free surface. The method is far more efficient than the second-order finite difference method (FDM) in the determination of the unstable eigenvalues, requiring CPU times which are more than one or two orders of magnitude less than that of the FDM for a given accuracy. While the computational overhead to implement the GDQ method is higher than for the FDM, its very high-order accuracy implies that only a small number of grid points are required.

Our study indicates that wake flows near a free surface in water of infinite depth are convectively unstable at low Froude number and absolutely unstable at higher Froude number. (Specifically, $Fr \geqslant 4{\cdot}5$ for wake flows behind a hydrofoil and $Fr \geqslant 2{\cdot}6$ for wake flows behind a circular cylinder.) These results are in good agreement with the findings of Triantafyllou and Dimas[5] and Dimas.[11]

Our analysis of the effect of depth on the linear stability of the wake flow downstream of a half-submerged body assuming the shape of a hydrofoil and a circular cylinder indicates that it has a limited influence on the nature of the instability. Comparison made with the reference 'infinite' depth case for cases with depth $h \geqslant 2$ only shows a variation of at most 20% in the critical ω_{0i}. The corresponding maximum temporal growth rate $(\omega_i)_{max}$ for the different depths also has variation of less than 20%.

REFERENCES

1. W. Koch, 'Local instability characteristics and frequency determination f self-excited wake flows', *J. Sound Vibr.* **99**, 53–83 (1985).
2. G. E. Mattingly and W. O. Criminal, 'The stability of an incompressible two-dimensional wake', *J. Fluid Mech.*, **51**, 233–272 (1972).
3. P. A. Monkewitz, 'The absolute and convective nature of instability in two-dimensional wakes at low Reynolds numbers', *Phys. Fluids*, **31**, 999–1006 (1988).
4. G. S. Triantafyllou, M. S. Triantafyllou and C. Chryssoslomidis. 'On the formation of vortex streets behind stationary cylinders', *J. Fluid Mech.*, **170**, 461–477 (1986).
5. G. S. Triantafyllou and A. A. Dimas, 'Interactin of two-dimensional separated flows with a free surface at low Froude numbers', *Phys. Fluids A*, 1813–1821 (1989).
6. C. Shu and B. E. Richards, 'Generalized differential quadrature and its application', *Aero Rep. 9117*, Glasgow University, 1991.
7. R. Bellkman, B. G. Kashef and J. Casti, 'Differential quadrature: a technique for the rapid solution of nonlinear partial differential equations', *J. Comput. Phys.*, **10**, 40–52 (1972).
8. P. G. Drazin and W. H. Reid, *Hydrodynamics Stability*, Cambridge University Press, Cambridge, 1981.
9. A. Bers, *Handbook of Plasma Physics*, North-Holland, Amsterdam, 1983.
10. K. Kupfer, A. Bers and A. K. Ram, 'The cusp map in the complex-frequency plane for absolute instabilities', *Phys. Fluid*, **30**, 3075–3082 (1987).
11. A. A. Dimas, 'Interactin between a two-dimensional wake and the free surface at low Froude number', *Master Thesis*, Massachusetts Institute of Technology, 1988.
12. B. J. Cantwell, 'A flying hot-wire study of the turbulent wake of a circular cylinder at a Reynolds number of 140,000', *Ph.D. Thesis*, California Institute of Technology, 1976.

